A Novel Form of the Plasminogen Activator Inhibitor Created by Cysteine Mutations Extends Its Half-Life: Relevance to Cancer and Angiogenesis[1]

Joanna Chorostowska-Wynimko,[2] Rafal Swiercz,[3] Ewa Skrzypczak-Jankun, Adam Wojtowicz, Steven H. Selman, and Jerzy Jankun[4]

Medical College of Ohio, Urology Research Center, Department of Urology [J. C-W., R. S., E. S-J., A. W., S. H. S., J. J.], and Department of Physiology and Molecular Medicine, [J. C-W., S. H. S., J. J.], Toledo, Ohio 43614-5807

Abstract

Proteolytic activity driven by urokinase (uPA) is commonly recognized as an important factor in metastasis and angiogenesis. The eradication of unwanted uPA activity expressed by cancer cells results in the inhibition of metastasis and angiogenesis. Development of novel and highly selective uPA inhibitors could, therefore, produce new treatments of cancer. The ultimate goal of this work is the identification of novel and selective inhibitors of uPA suitable for this purpose. We have chosen plasminogen activator inhibitor(s) type 1 (PAI-1), which selectively inhibits the urokinase plasminogen activator (uPA). However, PAI-1 is not a stable molecule and converts itself into the latent form with a half-life in the range of $t_{1/2} = 1–2$ h. This conversion is associated with a partial insertion of the reactive loop (P4–P10′) into the PAI-1 molecule. In such a conformation, P1–P1′ and other sites are not accessible for reaction with uPA. To conquer this hurdle, we have produced several PAI-1 mutants by replacing chosen amino acids with cysteine in the hope of creating disulfide bridges, which could make this insertion more difficult. On the basis of the known structure of active PAI-1, we have identified amino acids that can be substituted with a cysteine residue to produce disulfide bridges linking the top and bottom parts of strands A3 and A5 as well as sites within the helix-D region. We created a total of seven cysteine mutants via point mutation (two to six point mutations), generating possible sites for disulfide bridge formation at the top and bottom parts of A3 and A5, within the helix-D region, or by a combination thereof. Desired mutations were introduced by PCR using appropriate primers. The mutant forms of PAI-1 containing the chitin-binding intein tag were then purified using affinity chromatography wherein the intein tag is cleaved, leaving mutant PAI-1 protein. Cys mutations resulted in proteins with extended half-life of PAI-1 from 2 to >700 h depending on the mutant. Novel PAI-1 were fully functional against uPA and showed activity in the *in vitro* model of angiogenesis, *e.g.,* in the inhibition of sprout formation. Such prolonged serpin activity, which is therapeutically desired in cancer treatment and Cys-mutated PAI-1, could launch a new class of novel anticancer agents.

Introduction

Proteolytic activity driven by uPA[5] or metalloproteases is commonly recognized as an important factor in metastasis and angiogenesis. The uPA system contains the following elements: (*a*) plasminogen; the enzyme in its nonactive form is called plasminogen and in the active form is called plasmin. Plasmin is a strong proteolytic enzyme, and it activates other latent proteolytic enzymes also, broadening the spectrum of proteins attacked. Plasmin is a key enzyme in the tumor invasion and the development of distant metastasis; (*b*) activators: uPA and tPA. Both are weak proteolytic enzymes that activate plasminogen into plasmin by proteolytic cleavage. uPA is involved in pericellular proteolysis under a variety of physiological and pathological conditions. tPA mediates mainly intravascular thrombolysis (1–8); (*c*) inhibitors of plasminogen activators; there are four known inhibitors of uPA: PAI-1, PAI-2, PAI-3, and a protein called nexin. Most relevant in the metastatic process is PAI-1; (*d*) the binding site of uPA is called the uPAR. High numbers of uPARs on the surface of cells, if occupied by uPA, create high proteolytic activity in the proximity of cancer cells (9, 10).

An increased amount or activity of uPA, or uPAR per cell, has been found in human cancer cell lines with metastatic behavior (11). Moreover, animals that receive injections of PC3 prostatic cancer cells expressing higher amounts of uPA and/or uPAR develop metastatic lesions, including skeletal metastasis, earlier and more frequently than animals that receive injections

of the same cells expressing lower amounts of uPA/uPAR (10). The other plasminogen activator, tPA, does not seem to be relevant in the metastatic process (12).

The ability of human carcinoma cells (expressing uPA) to invade the chorioallantoic membrane and metastasize from it to the embryo, while treated with the antibody against the active site of uPA, was dramatically reduced in comparison with nontreated cells in the chicken embryo model (7). Cells transfected with a uPA plasmid, overexpressing in prostate cancer cells, showed an increase in metastasis, in comparison with the parental cell phenotype in the rat model. From the same phenotype, the cells underexposing uPA were selected, and these cells displayed a drastically decreased metastasis including skeletal metastasis (9).

It has been shown recently that inhibitors of uPA could reduce tumor size. Billstrom *et al.* (13) showed that *p*-aminobenzamidine, a competitive inhibitor of uPA, caused dose-dependent inhibition of uPA activity and decreased tumor growth in DU-145 (human prostate cancer cells)-inoculated SCID mice, when compared with nontreated animals. Amiloride, another uPA inhibitor, reduces tumor growth and decreases the proliferation of the tumor cells in the hepatomas and intestinal carcinomas and LnCAP prostatic cancer xenografts grown in SCID mice (14–18).

It has been reported that the reduction of cancer growth by uPA inhibitors is related to antiangiogenic activity (19, 20). The tip of neovascular advancing capillary vessels surrounding tumors has been reported to contain high amounts of uPA and its receptor. Binding of the proteolytically inactive ligand to uPAR reduces the amount of uPA on the surface of capillary endothelial cells and reduces tumor growth. Also, our studies have shown that uPA inhibitors reduce angiogenesis in the chicken embryo model, reducing the length and number of sprouts of HUVEC cells (19). In both cases, the inhibition of uPA activity on the tip of the capillary vessel or sprout prohibits cell migration and reduces cell growth. Eradication of unwanted uPA activity expressed by cancer cells results in the inhibition of metastasis and uPA-driven angiogenesis. Development of novel and highly selective uPA inhibitors could, therefore, produce new treatment of cancer. The ultimate goal of this work was an identification of novel and selective inhibitors of uPA suitable for cancer treatment. Most of the small chemical inhibitors are toxic in uPA-inhibitory activity, and frequently, they inhibit other serine proteases. Therefore, we have chosen PAI-1, which selectively inhibits activators of plasminogen. However, PAI-1 is not a stable molecule and converts itself into the latent form with a half-life in the range of $t_{1/2} = 1$–2 h. This conversion is associated with partial insertion of the reactive loop (P4–P10′) into the PAI-1 molecule. In such conformation, P1–P1′ and other sites are not accessible for reaction with uPA. To conquer this hurdle, we have produced several PAI-1 mutants, replacing chosen amino acids with Cys in the hope of creating disulfide bridges, which could make this insertion more difficult. Cys mutations resulted in proteins with extended half-life of PAI-1

from 2 to >700 h. Such prolonged activity could be therapeutically desired in cancer treatment.

Materials and Methods
Obtaining the Starting Structure
All of the molecular modeling and structure visualizations were done on a Silicon Graphics, Inc. workstation using the InsightII program package from Molecular Structure Inc., San Diego, CA. Atomic coordinates of latent and active PAI-1 were retrieved from the Protein Data Bank [entries 1C5G (21) and 1B3K (22)]. Hydrogen atoms were added and appropriate charges assigned throughout the PAI-1 molecules assuming the physiological pH to be 7.4.
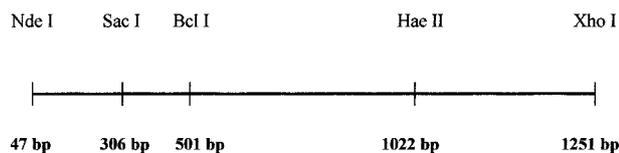
Molecular Modeling of Cys PAI-1 Mutants
To produce theoretical PAI-1 protein structure, all of the possible mutant sequences were sent to SWISS-MODEL (Automated Protein Model Server, http://www.expasy.org/swissmod/SWISS-MODEL.html; Refs. 23 and 24). The theoretical model was based on the known structure of active PAI-1 (1B3K). Energy minimization calculations for Cys 192 and Cys 347 were done using the InsightII program. After making −S-S- bond between these cysteines, PAI-1 was subjected to potential energy minimization calculations for 100 cycles. The following parameters were used: radius of subset from Cys 192, 8 Å; MC temperature, 20; and energy tolerance, 5000. After this step, the structure underwent simulated annealing from 500 K to 300 K in 10 K steps with molecular dynamics for 10 fs in each step. Finally, the structure was minimized again for 2500 cycles.

Expression of PAI-1
The human PAI-1 cDNA (from D. Ginsburg, University of Michigan, Ann Arbor, MI) was excised from the pQE30-PAI-1 vector as a *Nde*I/*Nsi*I fragment and separated from the pQE30 vector by DNA agarose gel electrophoresis. The PAI-1 cDNA was further cut to a *Nde*I/*Pst*I fragment and removed from gel by electroelution. This fragment was then ligated using the T4 DNA ligase into the *Nde*I/*Pst*I-cut pTYB-12 vector to create pTYB12-PAI-1 vector and was transformed into *Escherichia coli* strain ER2567 by rubidium chloride precipitation. Transformed cells were seeded on nutrient agar plates containing ampicillin (100 μg/ml) and grown overnight at 37°C. Next, a single colony was transferred to a test tube containing 6 ml of LB-broth and ampicillin and grown overnight. On the following day, pTYB12-PAI-1 plasmid DNA was isolated using the alkaline lysis method. Purified plasmid DNA was subjected to restriction analysis to determine that PAI-1 cDNA was incorporated into the pTYB12 vector by double digestion with *Nde*I and *Blp*I restriction enzymes. Finally, pTYB12-PAI-1 plasmid DNA was transformed by rubidium chloride precipitation into ER2566 *E. coli* strain, which has *T7 polymerase* gene incorporated into its genome. All uPA PAI-1 were constructed and expressed in the same way.

Design of Cys PAI-1 Mutants

The cDNA encoding PAI-1 was excised from the pQE30-PAI-1 plasmid as a *Nde*I/*Nsi*I fragment. The PAI-1 cDNA was divided into four sections as follows:

```
Nde I      Sac I    Bcl I                    Hae II              Xho I


├──────────┼────────┼────────────────────────┼──────────────────┤

47 bp      306 bp   501 bp                   1022 bp            1251 bp
```

Fragment *Nde*I/*Sac*I (259 bp long) was used to introduce mutations Val8→Cys and Ala74→Cys by PCR mutational analysis using forward primer: 5′-TAAGAAGGAGATAT-ACATATGGTGCACCATCCCCCATCCTACTGTGCCCACCT-GGCCTCA-3′; and reverse primer: 5′-TCCATGGCCCCAT-GAGCTCCTTGTACAGATGCCGGAGGCAGGGGGCCATG-3′.

Afterward, the PCR product was digested with *Nde*I and *Sac*I restriction enzymes and ligated into *Nde*I/*Sac*I-cut pCITE-PAI-1 to yield helix-D mutant. Subsequently, helix-D PAI-1 cDNA was transferred as a *Nde*I/*Xho*I fragment into the previously cut *Nde*I/*Xho*I pTYB12 vector.

Fragment *Bcl*I/*Hae*II (521 bp long) was used to introduce mutations: Leu169→Cys alone, Gln174→Cys alone, and Leu169→Cys and Gln174→Cys together using DNA oligonucleotides.

Lastly, the PCR product was digested with *Hae*II and *Xho*I restriction enzymes and was ligated with *Bcl*I/*Hae*II wild-type PAI-1 fragment into *Bcl*I/*Xho*I-cut pCITE-PAI-1 vector.

To create the β-sheet top clone, the Gln174→Cys mutant fragment *Bcl*I/*Hae*II with the Gly332→Cys fragment *Hae*II/*Xho*I were ligated into *Bcl*I/*Xho*I-cut wild-type pCITE-PAI-1 vector, and, subsequently, the entire *Nde*I/*Xho*I cDNA fragment was transferred into previously cut *Nde*I/*Xho*I pTYB12 vector.

To create the β-sheet bottom clone, the Leu169→Cys mutant fragment *Bcl*I/*Hae*II with the Val324→Cys fragment *Hae*II/*Xho*I were ligated into the *Bcl*I/*Xho*I-cut wild-type pCITE-PAI-1 vector, and, subsequently, the entire NdeI/XhoI cDNA fragment was transferred into previously cut *Nde*I/*Xho*I pTYB12 vector.

To create the β-sheet top and bottom clone, containing Leu169→Cys, Gln174→Cys, Val324→Cys, and Gly332→Cys together, the fragments *Bcl*I/*Hae*II and *Hae*II/*Xho*I were ligated into the *Bcl*I/*Xho*I-cut wild-type pCITE-PAI-1 vector. Subsequently, the entire *Nde*I/*Xho*I cDNA fragment was transferred into the previously cut *Nde*I/*Xho*I pTYB12 vector.

To create the helix-D and β-sheet top clone, the *Bcl*I/*Xho*I fragment from β-sheet top clone was ligated into *Bcl*I/*Xho*I-cut pCITE PAI-1 HELIX-D plasmid DNA. Subsequently, the entire *Nde*I/*Xho*I cDNA fragment was transferred into previously cut *Nde*I/*Xho*I pTYB12 vector.

To create the helix-D and β-sheet bottom clone, the *Bcl*I/

```
forward: 5’-ACAAAAGGTATGATCAGCAACTTGCTTGGGAAAGGAGCCGTGGACCAGCTGACA

         CGGCTGGTGCTGGTGAATGCCTGCTACTTCAACGGCTGTTGGAAGACTCCCTTC-3’,

                              CT               CAG
reverse: 5’-CGATCTTCACTTTCTGCAGCGCCTGCG CGACGTGGAGAGG -3’
```

Next, the PCR product was digested with *Bcl*I and *Hae*II restriction enzymes and was ligated with a *Hae*II/*Xho*I wild-type PAI-1 fragment into the *Bcl*I/*Xho*I-cut pCITE-PAI-1 vector.

Fragment *Hae*II/*Xho*I (229 bp long) was used to introduce mutations: Val324→Cys alone, Gly332→Cys alone, and Val324→Cys and Gly332→Cys together, using DNA oligonucleotides.

*Xho*I fragment from the β-sheet bottom clone was ligated into *Bcl*I/*Xho*I-cut pCITE PAI-1 HELIX-D plasmid DNA. Subsequently, the entire *Nde*I/*Xho*I cDNA fragment was transferred into the previously cut *Nde*I/*Xho*I pTYB12 vector.

To create the helix-D and β-sheet top and bottom clone, the *Bcl*I/*Xho*I fragment from the β-sheet top and bottom clone was ligated into *Bcl*I/*Xho*I-cut pCITE PAI-1 HELIX-D plasmid DNA. Subsequently, the entire *Nde*I/*Xho*I cDNA frag-

```
forward: 5’-CCTCTCCACGTCGCGCAGGCGCTGCAGAAATGCAAGATCGAGGTGAACGAGAGTTGCACGGTGGCCTCCT-3’

                                   GTG                        G
reverse: 5’-TCTTTCCCGATGCATCTCGAGTTTTGTCCCAGATG-3’
```

ment was transferred into the previously cut NdeI/XhoI pTYB12 vector.

DNA Sequencing

The DNA sequence of the Cys mutants of human PAI-1 was determined using the Sanger (dideoxy) method (25). For the sequencing, we used two forward primers, 5′-CCCGAAA-AGTGCCACCTG-3′, and 5′-AGTGGACTTTTCAGAGGTG-GAG-3′ and two reverse primers, 5′-GTTCTGAGGTCAT-TACTGG-3′, and 5′-GTCGGTCATTCCGACGTTCT-3′.

In this method, pTYB12-PAI-1 plasmid DNA solution was added with the primer solution, deoxynucleotide mix, thermosequenase DNA polymerase solution and one of four ^{33}P-radiolabelled dideoxynucleotide solutions. The reaction was cycled for 60 min as follows: 95°C for 30 s; 55°C for 30 s; 72°C for 60 s. Reactions were terminated by the addition of Stop solution (95% formamide, 20 mM EDTA, 0.05% bromphenol blue, and 0.05% xylene cyanol FF). Samples were heated at 70°C for 5 min before electrophoretic size fractionation on polyacrylamide gels in GATC order, followed by autoradiography. The DNA sequence of Cys PAI-1 was read manually, and determined sequences were aligned using CloneMap software (Version 2.11; CGC Scientific, Inc., Ballwin, MO) to determine the entire DNA sequence of Cys PAI-1.

Purification of wPAI-1 and Cys PAI-1

One liter of fresh LB broth medium containing ampicillin was inoculated with freshly grown culture and was incubated at 37°C until the $A_{600 nm}$ of the cell culture reached 0.6. The expression of the PAI-1 was stimulated by the addition of isopropyl β-D-1-thiogalactopyranoside (IPTG) to a final concentration of 0.5 mM. Next, cells were spun down, the cell pellet was washed with 50 ml of ice-cold cell lysis buffer [20 mM Na-HEPES, 500 mM NaCl, 1 mM EDTA, 20 μM PMSF, 5 mM MgCl₂, and 10 μg/ml protease-free DNase (pH 8.00)]. After washing, cells were resuspended in 30 ml of cell lysis buffer and broken down in a French press. The cell debris was removed by centrifugation, and clear crude cell extract was transferred to a new tube and stored in the freezer at −20°C.

PAI-1 were isolated on an intein binding column. In this protocol, 30 ml of chitin bead resin were equilibrated with 10 bed volumes of column buffer [20 mM HEPES, 500 mM NaCl, and 1 mM EDTA (pH 8.00)]. Crude cell extract from 1 liter of cell culture was applied onto chitin bead column at a 0.5-ml/min flow rate. In the next step, the column was extensively washed with 20 bed volumes of column buffer at 1.0-ml/min flow rate to remove unbound proteins. Next, the column was fast flushed with three bed volumes of cleavage buffer [20 mM HEPES, 500 mM NaCl, 1 mM EDTA, and 50 mM DTT (pH 8.00)] at 2.0 ml/min and incubated for 40 h at 4°C to stimulate on-column cleavage. The release from intein purification tag PAI-1 were eluted from the column with column buffer and and collected in 8-ml fractions. The eluted PAI-1 was dialyzed overnight against PBS buffer [120 mM NaCl, 2.7 mM KCl, and 10 mM Na₃PO₄ (pH 7.40)] and concentrated. Yield was ~1–2 mg per 1 liter of cell culture.

PAI-1 were further purified using centrifugal Vivapure D spin columns (Vivascience, Sartorius, Inc., Germany). These columns separate proteins based on their pI. Proteins were diluted in loading buffer [25 mM Tris/HCl (pH = 8.00)] and applied on the column previously equilibrated with the same buffer. Columns were spun for 5 min at 500 × g to remove contaminating proteins. Subsequently, columns were washed twice with the loading buffer. Pure PAI-1 protein was obtained by step salt elution [0.25× 1 M NaCl in 25 mM Tris/HCl (pH 8.00)]. Eluted PAI-1 was concentrated on the centrifugal filters with a membrane of M_r 5000 cutoff (Vivascience) in PBS to desired concentration. PAI-1 was used immediately after purification or was frozen (−20°C) only one time before use.

Protein Sequencing

Protein sequencing was done at the Protein Structure Facility of the University of Michigan at Ann Arbor on the Applied Biosystems (ABI) Model 420H instrument using standard procedure.

Western Blot Analysis

Crude cell extract and purified PAI-1 in loading buffer [0.5 M Tris-HCl (pH = 6.80), 10% glycerol, 10% SDS, 0.1% bromphenol blue, and 2.7 mM β-mercaptoethanol] were subjected to SDS-PAGE (10% gel). The gel was equilibrated in transfer buffer (20% methanol, 193 mM glycine, and 25 mM Tris-HCl) for 5 min after the run and proteins from the polyacrylamide gel were transferred to a nitrocellulose membrane (0.45 μm) at 100 V for 2 h. The nitrocellulose membrane was then washed in blotting buffer [PBS (pH 7.40), and 0.05% Tween 20), blocked in 5% nonfat milk in blotting buffer for 1 h at room temperature, and washed. The membrane was then treated with primary goat antihuman PAI-1 antibody (5 μg/ml in blotting buffer containing 1% BSA) for 1 h at room temperature and washed. This was followed by treatment with secondary horseradish peroxidase-conjugated antigoat antibody (1:2000 dilution, in blotting buffer containing 1% BSA) for 1 h at room temperature and washed. Finally, the membrane was incubated in horseradish peroxidase substrate solution (metal enhanced 3,3′-diaminobenzidine tetrahydrochloride, 1:10 dilution) for 15 min at room temperature. After stopping the reaction by rinsing with deionized water, the membrane was allowed to air-dry.

uPA/PAI-1 Complex Formation Assay

In this assay, 20 μl of uPA solution {2.0 mg/ml stock solution in coupling buffer [50 mM Na₃PO₄, 150 mM NaCl, and 1 mM EDTA (pH 7.00)]} was mixed with 40, 50, and 60 μl of PAI-1 solution (2 mg/ml stock solution in coupling buffer) and incubated for 30 min at room temperature. Samples were then mixed with a loading buffer and subjected to SDS-PAGE under nonreducing conditions. After the run, polyacrylamide gel was stained in staining solution for 20 min at room temperature followed by overnight destaining in destaining solution.

PAI-1 Activity Determination

PAI-1 specific inhibitory activity was measured by a chromogenic assay. Serial dilutions (0.22–1.35 nM) of PAI-1 in activity assay buffer (150 mM NaCl, 50 mM Tris-HCl (pH 7.5), and 100 μg/ml BSA) were mixed with an equal volume of 50 IU/ml LMW uPA (American Diagnostica, Inc., Greenwich, CT) and incubated at the room temperature for 30 min. Afterward, the residual activity was determined by the addition of the substrate (SPECTROZYME-UK) to a final concentration of 0.17 mM, and absorbency was measured at 405 nm every 30 s for 15 min. The concentration of active PAI-1 was calculated from the amount of sample that inhibited the uPA activity by 50% as compared with samples containing uPA alone.

Inhibitory Constant (K_i). K_i was determined by chromogenic assay using the serial dilutions of SPECTROZYME-United Kingdom (American Diagnostica, Inc.) as substrate. Equal volumes of PAI-1, LMW uPA (12.5 IU/ml) and SPECTROZYME-United Kingdom solutions in reaction buffer [50 mM Tris (pH 8.80) and 0.01% Tween 80] were mixed and incubated for 15 min at the room temperature. Afterward, absorbency was determined at 405 nm. K_i was determined using Lineweaver-Burk plot.

Determination of the Half-Life Time of PAI-1 Mutants. PAI-1 proteins diluted in Activity Assay buffer [150 mM NaCl, 50 mM Tris (pH 7.5), and 100 μg/ml BSA] were incubated at room temperature. The activity of PAI-1 proteins was determined by chromogenic assay. The equal volume (50 μl) of LMW u-PA (50 IU/ml) and SPECTROZYME-United Kingdom (American Diagnostica, Inc.) substrate (100 μl) was added after 30 min incubation in room temperature, and the absorbance at 405 nm was measured every 15 s for 15 min. The percentage of uPA inhibition by PAI-1 was calculated as a percentage change between the rate of the reaction in control and PAI-1-containing wells. The percentage of PAI-1 activity was plotted *versus* time, and the data set was fitted into a single exponential equation ($y = ae^{-bx}$, where a is an amplitude and b is the decay constant, k_{obs}). The half-life time was calculated using the equation $t_{1/2} = (\ln 2)/k_{obs}$.

Cell Line, Cell Culture Conditions, and Sprout Formation Assay

The human vascular endothelial cell line HUVEC was purchased from Cambrex, Inc., East Rutherford, NJ. HUVECs were grown to confluence in EGM-2 MV growth medium. Next, cells were trypsinized and seeded onto 0.5% agarose-coated culture dishes. This procedure resulted in a cell aggregate formation after 24 h of incubation at 37°C. The HUVEC aggregates were incubated for 30 min at room temperature. The old-medium supernatant was decanted, and HUVEC aggregates were suspended in 5 ml of fresh EGM-2 MV growth medium.

Three-dimensional fibrin gels were prepared by mixing the following in 12-well culture plates: 960 μl of human fibrinogen (type III, 60% of protein clottable; 2.50 mg/ml concentration in RPMI 1640), 40 μl of HUVEC aggregate suspension, and 12.5 μl of human thrombin (25 units/ml concentration in RPMI 1640). The mixture was mixed and allowed to gel for about 4 min at 37°C before adding EGM-2

MV growth medium over the gel. The HUVEC aggregates were suspended in fibrin gel containing Cys PAI-1, and 1 ml of EGM-2 MV growth medium was added over the fibrin gel. The PAI-1 in the fibrin gel was adjusted to final concentrations of 0.75, 1.50, and 3.00 μM. The Cys PAI-1 mutant solution used in this study was dialyzed against PBS buffer (pH 7.40) overnight at 4°C. After 3 days of cell incubation, cultures were fixed *in situ* for 24 h with 2 ml of 10% formalin solution and photographed under a phase-contrast microscope.

Image Processing and Analysis

The measurement of sprout length was performed by a dedicated image recognition algorithm implemented in the C++ programming language and a software application that was build using Microsoft Visual C++ 6.0 and the CImage graphics library. Digital microscope images of sprouts were used as input values. On analyzed images, sprouts are thin, long or short objects, usually slightly darker than the background. Sprouts were detected automatically based on their gradient of gray intensity and morphology. Sprouts were extracted by the size filter (too-small objects were removed) and by the shape filter (too-round objects were removed). When all of the remaining objects on the image could be considered as sprouts, the approximate algorithm of determining skeletons of the objects was applied. The skeleton is the part of an object that largely preserves the extent and the connectivity of the original area while removing most of the original foreground points. The length of a given sprout was defined by the size of its skeleton in pixels.

The algorithm described above returns as a result the length of each sprout and total values calculated from a single two-dimensional image. However, sprouts are three-dimensional objects; therefore, several subsequent two-dimensional images of one aggregate were analyzed. An average value of the length of one aggregate was obtained. Finally, an average value of sprouts length for each mutated PAI-1 in given concentration was determined. We measured at least five different aggregates for each concentration of different PAI-1. The number of measurements was usually higher than five because some aggregates were measured several times at different depths of the microscope field.

Results

Design of Cys PAI-1 Mutants. Active PAI-1 has a reactive loop containing a P1–P1′ site that can extend up to 18 Å from the body of the molecule, whereas, in latent PAI-1, this loop is placed between the A3 and A5 strands of the corresponding β-sheet rendering the P1–P1′ site inaccessible to uPA. By restraining the movement of the A3 and A5 strands, as well as limiting the flexibility of the helix-D region, it might be possible to prevent insertion of the reactive loop between A3 and A5 and, hence, extend the $t_{1/2}$ of PAI-1. On the basis of the known structure of active PAI-1, we have identified amino acids that can be substituted with a Cys residue to produce disulfide bridges linking the top and bottom parts of strands A3 and A5, as well as sites within the helix-D region. A total of seven Cys mutants (two to six point mutations, with an
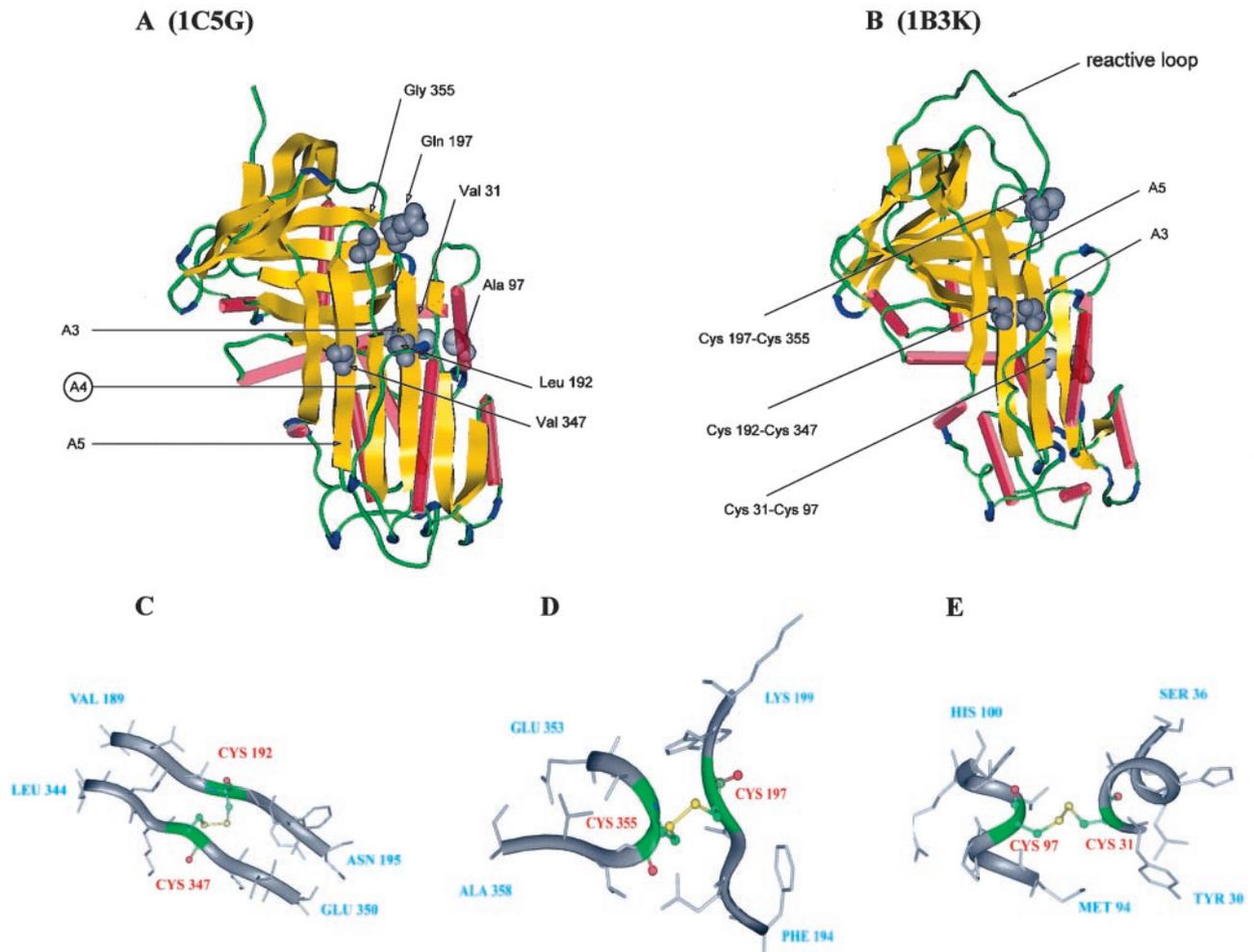
Fig. 1. *A* and *B*, a ribbon model of inactive (*A*, *1C5G*) and active (*B*, *1B3K*) PAI-1; *green*, strands; *yellow*, β-sheets; *red*, α-helices. *Gray CPK spheres*, mutated amino acids. *C*, *D*, and *E*, a ribbon model of disulfide bridges of Cys PAI-1 mutants (*C*, β-sheet bottom; *D*, β-sheet top; *E*, helix-D mutations). Atom types color coded for cysteines only: *green*, carbons; *yellow*, sulfurs; *red*, oxygens. For clarity, hydrogen atoms are not shown.

even number of cysteines) can generate possible sites for the disulfide bridge formation at the top and bottom parts of A3 and A5, within the helix-D region, or by a combination thereof (Fig. 1, *A* and *B*). We chose the following mutations, which could produce disulfide bridges: the Cys 31–Cys 97 (helix-D) bridge reduces the flexibility of PAI-1 molecule by holding together N-terminus to the nearest helix; the Cys 192–347 (β-sheet bottom) bridge tightly holds the A3-A5 strands, and most upper one: the Cys 197–Cys 355 (β-sheet top) ends stiffen the reactive loop and prevent its backtracking into the β sheet.

Models of mutated PAI-1 returned from SWISS-MODEL showed disulfide bridges in all of the mutants in helix-D and β-sheet top regions, but not in β-sheet bottom. The distance between sulfur atoms on modeled proteins was too big to form a bridge (7.41 Å). However, when models with this mutation were subjected to energy minimization, the cysteines in this region came closer and could produce a stable bridge as well (Fig. 1, *C*, *D*, and *E*).

Expression and Purification of Cys PAI-1. The Cys PAI-1 genes were inserted into the plasmid as described in the "Materials and Methods" section. To verify, mutations of all of the Cys PAI-1 genes were sequenced. Analysis of the DNA sequence of Cys PAI-1 mutants of the human PAI-1 revealed all of the mutations sites as expected (Fig. 2).

PAI-1, purified on a column in a single-step purification process, was analyzed by SDS-PAGE. Coomassie-Brilliant-Blue staining of the eluted fractions from the chitin beads column showed that fractions 3–5 revealed two dominant bands of M_r 43,000 and 78,000. The lower band of M_r 43,000 represents the molecular weight of recombinant PAI-1. By densitometric measurements of bands intensity on PAGE gel the M_r 43,000 band represents 70.7%, the M_r 78.000 represents 26.7% and, of three additional proteins in various molecular weights, 2.7%. M_r 78,000 is close enough to M_r 86,000 to raise the possibility that this band could be dimerized Cys PAI-1. To verify this possibility, we further analyzed crude and purified protein preparations. The immunostaining

```
          1         *        20         *        40         *        60
wild    PAI-1 1  ---------- ---------- ---VHHPPSY VAHLASDFGV RVFQQVAQAS KDRNVVFSPY
βst     PAI-1 1  ---------- ---------- ---VHHPPSY VAHLASDFGV RVFQQVAQAS KDRNVVFSPY
βsb     PAI-1 1  ---------- ---------- ---VHHPPSY VAHLASDFGV RVFQQVAQAS KDRNVVFSPY
hD      PAI-1 1  ---------- ---------- ---VHHPPSY CAHLASDFGV RVFQQVAQAS KDRNVVFSPY
hDβst   PAI-1 1  ---------- ---------- ---VHHPPSY CAHLASDFGV RVFQQVAQAS KDRNVVFSPY
hDβsb   PAI-1 1  ---------- ---------- ---VHHPPSY CAHLASDFGV RVFQQVAQAS KDRNVVFSPY
βstb    PAI-1 1  ---------- ---------- ---VHHPPSY VAHLASDFGV RVFQQVAQAS KDRNVVFSPY
hDβstb  PAI-1 1  ---------- ---------- ---VHHPPSY CAHLASDFGV RVFQQVAQAS KDRNVVFSPY
                                                        ↑
wild    PAI-1 61 GVASVLAMLQ LTTGGETQQQ IQAAMGFKID DKGMAPALRH LYKELMGPWN KDEISTTDAI
βst     PAI-1 61 GVASVLAMLQ LTTGGETQQQ IQAAMGFKID DKGMAPALRH LYKELMGPWN KDEISTTDAI
βsb     PAI-1 61 GVASVLAMLQ LTTGGETQQQ IQAAMGFKID DKGMAPALRH LYKELMGPWN KDEISTTDAI
hD      PAI-1 61 GVASVLAMLQ LTTGGETQQQ IQAAMGFKID DKGMAPCLRH LYKELMGPWN KDEISTTDAI
hDβst   PAI-1 61 GVASVLAMLQ LTTGGETQQQ IQAAMGFKID DKGMAPCLRH LYKELMGPWN KDEISTTDAI
hDβsb   PAI-1 61 GVASVLAMLQ LTTGGETQQQ IQAAMGFKID DKGMAPCLRH LYKELMGPWN KDEISTTDAI
βstb    PAI-1 61 GVASVLAMLQ LTTGGETQQQ IQAAMGFKID DKGMAPALRH LYKELMGPWN KDEISTTDAI
hDβstb  PAI-1 61 GVASVLAMLQ LTTGGETQQQ IQAAMGFKID DKGMAPCLRH LYKELMGPWN KDEISTTDAI
                                                       ↑
wild    PAI-1 121 FVQRDLKLVQ GFMPHFFRLF RSTVKQVDFS EVERARFIIN DWVKTHTKGM ISNLLGKGAV
βst     PAI-1 121 FVQRDLKLVQ GFMPHFFRLF RSTVKQVDFS EVERARFIIN DWVKTHTKGM ISNLLGKGAV
βsb     PAI-1 121 FVQRDLKLVQ GFMPHFFRLF RSTVKQVDFS EVERARFIIN DWVKTHTKGM ISNLLGKGAV
hD      PAI-1 121 FVQRDLKLVQ GFMPHFFRLF RSTVKQVDFS EVERARFIIN DWVKTHTKGM ISNLLGKGAV
hDβst   PAI-1 121 FVQRDLKLVQ GFMPHFFRLF RSTVKQVDFS EVERARFIIN DWVKTHTKGM ISNLLGKGAV
hDβsb   PAI-1 121 FVQRDLKLVQ GFMPHFFRLF RSTVKQVDFS EVERARFIIN DWVKTHTKGM ISNLLGKGAV
βstb    PAI-1 121 FVQRDLKLVQ GFMPHFFRLF RSTVKQVDFS EVERARFIIN DWVKTHTKGM ISNLLGKGAV
hDβstb  PAI-1 121 FVQRDLKLVQ GFMPHFFRLF RSTVKQVDFS EVERARFIIN DWVKTHTKGM ISNLLGKGAV
                                                        ↑
wild    PAI-1 181 DQLTRLVLVN ALYFNGQWKT PFPDSSTHRR LFHKSDGSTV SVPMMAQTNK FNYTEFTTPD
βst     PAI-1 181 DQLTRLVLVN ALYFNGCWKT PFPDSSTHRR LFHKSDGSTV SVPMMAQTNK FNYTEFTTPD
βsb     PAI-1 181 DQLTRLVLVN ACYFNGQWKT PFPDSSTHRR LFHKSDGSTV SVPMMAQTNK FNYTEFTTPD
hD      PAI-1 181 DQLTRLVLVN ALYFNGCWKT PFPDSSTHRR LFHKSDGSTV SVPMMAQTNK FNYTEFTTPD
hDβst   PAI-1 181 DQLTRLVLVN ALYFNGCWKT PFPDSSTHRR LFHKSDGSTV SVPMMAQTNK FNYTEFTTPD
hDβsb   PAI-1 181 DQLTRLVLVN ACYFNGCWKT PFPDSSTHRR LFHKSDGSTV SVPMMAQTNK FNYTEFTTPD
βstb    PAI-1 181 DQLTRLVLVN ACYFNGCWKT PFPDSSTHRR LFHKSDGSTV SVPMMAQTNK FNYTEFTTPD
hDβstb  PAI-1 181 DQLTRLVLVN ACYFNGCWKT PFPDSSTHRR LFHKSDGSTV SVPMMAQTNK FNYTEFTTPD
                                ↑    ↑
wild    PAI-1 241 GHYYDILELP YHGDTLSMFI AAPYEKEVPL SALTNILSAQ LISHWKGNMT RLPRLLVLPK
βst     PAI-1 241 GHYYDILELP YHGDTLSMFI AAPYEKEVPL SALTNILSAQ LISHWKGNMT RLPRLLVLPK
βsb     PAI-1 241 GHYYDILELP YHGDTLSMFI AAPYEKEVPL SALTNILSAQ LISHWKGNMT RLPRLLVLPK
hD      PAI-1 241 GHYYDILELP YHGDTLSMFI AAPYEKEVPL SALTNILSAQ LISHWKGNMT RLPRLLVLPK
hDβst   PAI-1 241 GHYYDILELP YHGDTLSMFI AAPYEKEVPL SALTNILSAQ LISHWKGNMT RLPRLLVLPK
hDβsb   PAI-1 241 GHYYDILELP YHGDTLSMFI AAPYEKEVPL SALTNILSAQ LISHWKGNMT RLPRLLVLPK
βstb    PAI-1 241 GHYYDILELP YHGDTLSMFI AAPYEKEVPL SALTNILSAQ LISHWKGNMT RLPRLLVLPK
hDβstb  PAI-1 241 GHYYDILELP YHGDTLSMFI AAPYEKEVPL SALTNILSAQ LISHWKGNMT RLPRLLVLPK
wild    PAI-1 301 FSLETEVDLR KPLENLGMTD MFRQFQADFT SLSDQEPLHV AQALQKVKIE VNESGTVASS
βst     PAI-1 301 FSLETEVDLR KPLENLGMTD MFRQFQADFT SLSDQEPLHV AQALQKVKIE VNESCTVASS
βsb     PAI-1 301 FSLETEVDLR KPLENLGMTD MFRQFQADFT SLSDQEPLHV AQALQKCKIE VNESGTVASS
hD      PAI-1 301 FSLETEVDLR KPLENLGMTD MFRQFQADFT SLSDQEPLHV AQALQKVKIE VNESGTVASS
hDβst   PAI-1 301 FSLETEVDLR KPLENLGMTD MFRQFQADFT SLSDQEPLHV AQALQKVKIE VNESCTVASS
hDβsb   PAI-1 301 FSLETEVDLR KPLENLGMTD MFRQFQADFT SLSDQEPLHV AQALQKCKIE VNESGTVASS
βstb    PAI-1 301 FSLETEVDLR KPLENLGMTD MFRQFQADFT SLSDQEPLHV AQALQKCKIE VNESCTVASS
hDβstb  PAI-1 301 FSLETEVDLR KPLENLGMTD MFRQFQADFT SLSDQEPLHV AQALQKCKIE VNESCTVASS
                                                         ↑           ↑
wild    PAI-1 361 STAVIVSARM APEEIIMDRP FLFVVRHNPT GTVLFMGQVM EP
βst     PAI-1 361 STAVIVSARM APEEIIMDRP FLFVVRHNPT GTVLFMGQVM EP
βsb     PAI-1 361 STAVIVSARM APEEIIMDRP FLFVVRHNPT GTVLFMGQVM EP
hD      PAI-1 361 STAVIVSARM APEEIIMDRP FLFVVRHNPT GTVLFMGQVM EP
hDβst   PAI-1 361 STAVIVSARM APEEIIMDRP FLFVVRHNPT GTVLFMGQVM EP
hDβsb   PAI-1 361 STAVIVSARM APEEIIMDRP FLFVVRHNPT GTVLFMGQVM EP
βstb    PAI-1 361 STAVIVSARM APEEIIMDRP FLFVVRHNPT GTVLFMGQVM EP
hDβstb  PAI-1 361 STAVIVSARM APEEIIMDRP FLFVVRHNPT GTVLFMGQVM EP
```
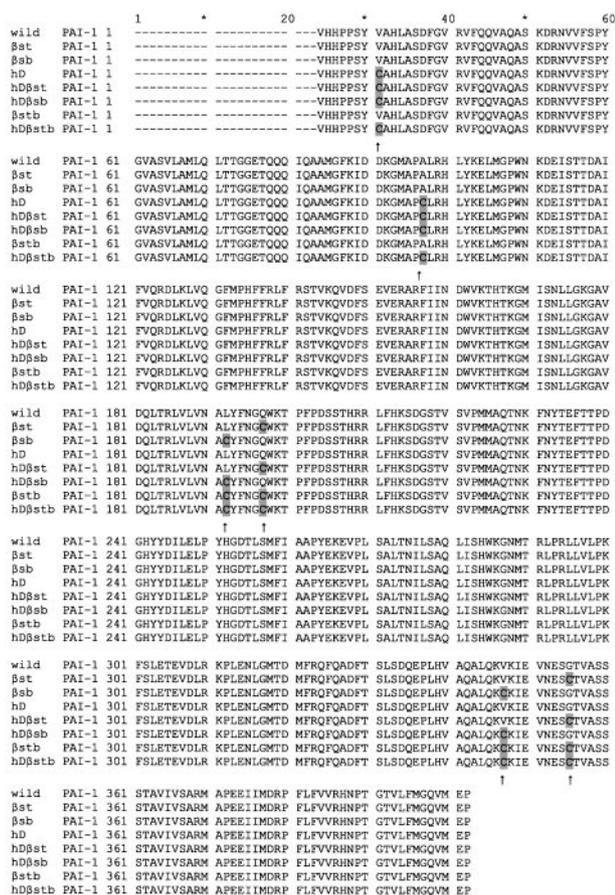
Fig. 2. The amino acid sequence of wild-type (*wild*) and Cys PAI-1. *Gray boxes*, Cys mutations. *βst*, β-sheet top; *βsb*, β-sheet bottom; *hD*, helix-D; *hDβst*, helix-D β-sheet top; *hDβsb*, helix-D β-sheet bottom; *βstb*, β-sheet top and bottom; *hDβstb*, helix-D β-sheet top and bottom.

```
                  1         *        20         *        40         *        60
78 kDa protein    -AAKDVKFGN DARVKMLRGV N-------- ---------- ---------- ----------
chaperone Hsp60   MAAKDVKFGN DARVKMLRGV NVLADAVKVT LGPKGRNVVL DKSFGAPTIT KDGVSVAREI
```
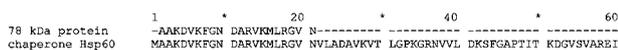
Fig. 3. The sequence of the first 20 amino acids of chaperone-like M_r 78,000 protein and the sequence of the first 60 amino acids of *E. coli* GroEL chaperone Hsp60. *kDa*, M_r in thousands.

Fig. 4. Inhibition of PAI-1 activity, for clarity only: ●, wild-type PAI-1 mutants; ■, helix-D β-sheet top PAI-1 mutants; ▲, β-sheet top PAI-1 mutants.

Table 1   Half-life time of cysteine PAI-1 mutations

Protein	Decay constant (k_{obs})	Half-life time (h)
w^a PAI	−0.4428	1.57
helix-D β-sheet tb PAI-1	−0.2967	2.34
helix-D PAI-1	−0.0315	22.00
helix-D β-sheet t PAI-1	−0.0109	63.59
helix-D β-sheet b PAI-1	−0.0076	91.20
β-sheet tb PAI-1	−0.0049	141.46
β-sheet b PAI-1	−0.0035	198.04
β-sheet t PAI-1	−0.0001	6931.47[b]

[a] w, wild type; t, top; b, bottom.
[b] This is the calculated value; we carried out measurements of activity for 700 h.

identified by immunostaining with anti-PAI-1 antibodies (data not shown).

As shown in Fig. 4 and Table 1, the inhibitory activity of mutated PAI-1 proteins declined over the time at different rates. Moreover, three different patterns of Cys PAI-1 activity decline could be observed. First, helix-D β-sheet top and bottom mutant activity deteriorated rapidly, and it was practically the same as that of wild-type PAI-1. Second, helix-D, helix-D β-sheet top, helix-D β-sheet bottom, β-sheet bottom and top, β-sheet bottom, mutants showed increased uPA-inhibitory activity, which varied considerably depending on the mutant. Third, the longest lasting activity was observed for β-sheet top PAI-1, which we measured up to 700 h. As shown in Table 1, the calculated half-life for this mutant could reach >6900 h.

For all future experimentation, we chose wild-type PAI-1, helix-D β-sheet top (intermediate half-life), and β-sheet top PAI-1 (the longest half-life). The inhibitory constants (K_i) of examined PAI-1 proteins were very similar to each other as determined by Lineweaver-Burke analysis. The value determined for wild-type PAI-1 was 1.38 10^{-7} M; for helix-D β-sheet top, 1.68 10^{-7} M; and for β-sheet top, 1.64 10^{-7} M. The specific inhibitory activity of wild-type PAI-1 and chosen Cys PAI-1 proteins against LMW uPA were very similar as well. The native form of PAI-1 exhibits 63.13 IU/µg. It was slightly lower for Cys PAI-1, 54.14 IU/µg for β-sheet top, and 50.17 IU/µg for helix-D β-sheet top.

Sprout Formation Inhibition by PAI-1. In our previous paper, we showed that the PAI-1 1B14 (26) mutant with

of nitrocellulose-attached proteins of crude protein extract revealed staining of M_r 90,000, which represents the fusion protein of intein/PAI-1, whereas fractions eluted from the column showed a band of M_r 43,000. No immunostaining was observed for the M_r 78,000 band. We also analyzed the amino acid sequence of the M_r 78,000 protein extracted from the PAGE gel. As shown in Fig. 3 (BLAST search), the first 20 amino acids of this protein are identical to the sequence of 2–21 amino acids of *E. coli* GroEL, chaperone Hsp60, and no similarity was found to the sequence of PAI-1. We, therefore, conclude that the M_r 78,000 band is not dimerized PAI-1.

Determination of PAI-1 Activity. The purified PAI-1 were active as determined by uPA/PAI-1 complex formation assay. For all three examined proteins, Coomassie-Brilliant-Blue staining of SDS-PAGE gel revealed a band of M_r 77,000 representing a stable LMW uPA/PAI-1 complex as positively
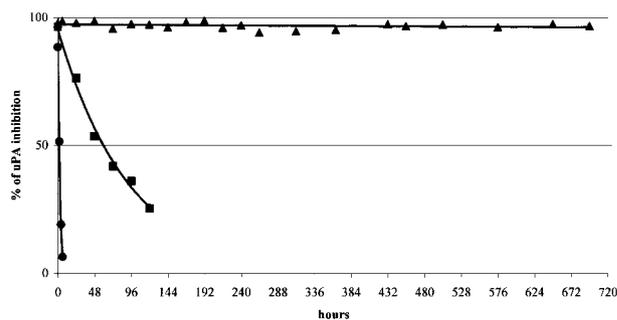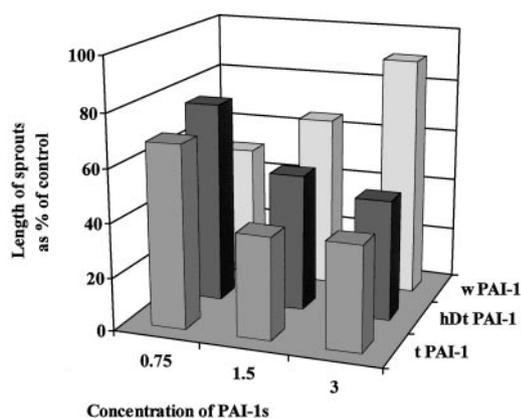
Fig. 5. Inhibition of HUVEC sprout formation by wild-type PAI-1 (*wPAI-1*) and Cys PAI-1 mutants (*hDt PAI-1*, *t PAI-1*). The effect of PAI-1 in fibrin gels is measured as the total length of sprouts in a single aggregate.

improved half-life inhibits sprout formation starting at concentration of 0.75 μM (19). Therefore, we used the same concentration as a starting point. The Cys PAI-1 reduced sprout formation in a concentration-dependent fashion as shown in Fig. 5. The most noticeable effect was observed in the case of mutant (β-sheet top), the one with the longest half-life. Less effective, as expected, was PAI-1 with a shorter half-life (helix-D β-sheet top). The wild-type PAI-1, with a very short half-life (1–2 h), instead of reducing sprout formation, induced it with an increase of concentration in the medium.

Discussion
The main goal of this work was to stabilize the active form of PAI-1 by introducing new disulfide bonds rather than salt bridges. Disulfide bridges stabilize proteins undergoing structural changes by decreasing the main chain entropy of their initial form (27, 28). The concept of stabilizing proteins by introducing cysteines that potentially form disulfide bridges was used successfully in the past. As an example, Ivens *et al.* (28) increased the thermal stability of ($\alpha\beta$)$_8$-barrel protein 13-fold over the native protein by linking two strains with a disulfide bond. Proteins expressed in *E. coli* usually require oxidation to promote formation of the disulfide bond. However, PAI-1 is sensitive to oxidative inactivation. The circular dichroism analysis revealed a rapid conformational change that correlated to the loss of uPA inhibitory activity. The oxidation sensitivity of PAI-1 was enhanced dramatically in the presence of 0.001% SDS, and the circular dichroism spectrum was significantly different from that of untreated PAI-1 (29). Therefore, we tried to avoid oxidative treatment of PAI-1. Spontaneous formation of disulfide bridges of *E. coli*-expressed proteins has been reported in several cases, especially if their number was no more that three (30, 31 and personal communication).[6] An increase of half-life time of different PAI-1 mutants could be, therefore, attributed to the

formation of disulfide bonds, as molecular simulations and three-dimensional structural modeling suggest.

After proteins were purified by chitin column, two strong bands were observed on SDS PAGE gel. Initially, we were concerned that the second band corresponded to dimerized PAI-1. Amino acid analysis revealed a strong homology of this band to GroEL of *E. coli*. Proteins are eluted from the chitin column dependent on their affinity to chitin. Apparently, GroEL of *E. coli* with the molecular weight of M_r 57,000–60,000 might have a high affinity to chitin and was reported to copurify with the protein of interest by Gibson *et al.* (32) and on the kit supplier home page (http://www.negb.com/neb/faqs/impact5.html). It was also suggested that this copurification might be a result of partial misfolding of the target protein that is still bound to GroEL, intein tag. The contaminating protein in our preparation has M_r 78,000, which supports the last assumption made. Nevertheless, molecular weights, Western blot data, amino acid sequence, as well as the above citation, exclude the possibility of intramolecular dimerization of PAI-1 by disulfide bridges.

Few attempts were made to extend the half-life of PAI-1 by introducing mutations to this protein. As an example Tucker *et al.* (21) mutated PAI-1 in the "gate" region (303Leu→Ile, 53Arg→Tyr) and achieved three times longer half-life of PAI-1. Similarly, Berkenpas *et al.* (26) achieved an even longer half-life with four point mutations (173Asn→His, 177Lys→Thr, 342Gln→Leu, 377Met→Ile) that delay the conversion of PAI-1 to the latent form by 145 h at 37°C. Some of these mutations were in the critical A3-A5 strands region forming salt bridges and hydrogen bonding. Our results are consistent with previous findings. Mutations in the helix-D region, which represents the lower part of the protein, named by Tucker *et al.* as gate produced a protein with a very similar half-life (21). The findings of Berkenpas *et al.* (26), as well as our double and single mutants in the A3, A5 region showed that this region is critical for significant extension of PAI-1 active half-life. None of the previous attempts produced PAI-1 with Cys disulfide bridges that would secure lasting, active PAI-1. Our results showed that only one disulfide bond is needed to extend the active half-life, and the most effective was the β-sheet top (197Gln→Cys, 355Gly→Cys) PAI-1 mutant. Somewhat puzzling are the results of six point mutations, in which cysteines should produce three disulfide bridges. PAI-1 should presumably generate a protein with the longest half-life given that all mutants with one or two disulfide bonds produce a protein that remains active longer that native PAI-1. This phenomenon could be the result of different folding of that mutant or the inability of that protein to form three disulfide bridges. Some unexpected results of PAI-1 mutations were also observed when amino acids were substituted into the reactive loop. Substitution in the P6 position (Val→Pro) revealed tPA target specificity, and P18 substitution (Asn→Pro) of PAI-1 exhibited inhibitory activity exclusively toward uPA (33).

The inhibitory activity of Cys PAI-1 were very similar to those of PAI-1 reported by Wagner *et al.* (62 IU/μg; Ref. 34) and by Lawrence *et al.* (52 IU/μg; Ref. 35). The determined inhibitory constant (K_i) of Cys PAI-1 was in the range of 1.3–1.7 10^{-7} M and was consistent with the results obtained

---

[6] Personal communication, Roche Applied Science.

by others (36, 37). These findings strongly suggest that Cys-mutated PAI-1 share structural similarities with wild-type PAI-1 and that the only changes in the protein molecule are disulfide bridges. However, the definite answer to this question will be possible only after completion of an ongoing structural study of Cys PAI-1.

It was demonstrated that PAI-1 is a potent regulator of angiogenesis and, hence, of tumor growth (19, 38). However, the application of PAI-1 in anticancer therapy was somewhat controversial. It has been shown on *in vitro* and *in vivo* models that, under certain conditions, PAI-1 could induce angiogenesis and tumor growth (20, 39). It was suggested that in some circumstances, vitronectin and PAI-1 act together *in vivo* either to promote or to inhibit angiogenesis. Vitronectin present in the provisional matrix might enhance angiogenesis by promoting vascular cell migration, and PAI-1, by controlling access to the integrin adhesion site on vitronectin, might regulate this process (40). However, it was shown in our previous studies and by others, that PAI-1 added at supraphysiological concentrations suppresses the vitronectin pathway and acts as a potent inhibitor of angiogenesis by using its inhibitory properties toward proteinase activity (19, 40). Sprout formation assay confirms these findings. Wild-type PAI-1, which looses its urokinase-inhibiting activity but preserves vitronectin-binding capacity, induces sprout formation in a concentration-dependent manner. By contrast, both PAI-1 with extended half-life (helix-D β-sheet top and β-sheet top mutants) reduce the ability of HUVEC cells to form sprouts. Furthermore, PAI-1 with the longest half-life was the most potent one. The appearance of the lesser inhibitory activity on sprout formation (Fig. 5) by the mutants at low concentration (0.75) might be uncertain because the only difference in higher concentrations were statistically significant ($P < 0.05$).

In conclusion, we want to emphasize that there were several attempts to use uPA inhibitors in anticancer and antiangiogenic therapy (14, 19, 40, 41). It seems that the most important in these therapies is preserving the serpin activity of PAI-1 for possibly the longest period of time, and the Cys β-sheet top PAI-1 mutant addresses this requirement.

Acknowledgments

References

1. Achbarou, A., Kaiser, S., Tremblay, G., Ste-Marie, L. G., Brodt, P., Goltzman, D., and Rabbani, S. A. Urokinase overproduction results in increased skeletal metastasis by prostate cancer cells *in vivo*. Cancer Res., *54:* 2372–2377, 1994.

2. Conese, M., and Blasi, F. Urokinase/urokinase receptor system: internalization/degradation of urokinase-serpin complexes: mechanism and regulation. Biol. Chem. Hoppe-Seyler, *376:* 143–155, 1995.

3. Conese, M., and Blasi, F. The urokinase/urokinase-receptor system and cancer invasion. Bailliere's Clin. Haematol., *8:* 365–389, 1995.

4. Festuccia, C., Vincentini, C., di Pasquale, A. B., Aceto, G., Zazzeroni, F., Miano, L., and Bologna, M. Plasminogen activator activities in short-term tissue cultures of benign prostatic hyperplasia and prostatic carcinoma. Oncol. Res., *7:* 131–138, 1995.

5. Festuccia, C., Dolo, V., Guerra, F., Violini, S., Muzi, P., Pavan, A., and Bologna, M. Plasminogen activator system modulates invasive capacity and proliferation in prostatic tumor cells. Clin. Exp. Metastasis, *16:* 513–528, 1998.

6. Ossowski, L., and Reich, E. Antibodies to plasminogen activator inhibit human tumor metastasis. Cell, *35:* 611–619, 1983.

7. Ossowski, L. *In vivo* invasion of modified chorioallantoic membrane by tumor cells: the role of cell surface-bound urokinase. J. Cell Biol., *107:* 2437–2445, 1988.

8. Wilson, M. J., and Sinha, A. A. Plasminogen activator and metalloprotease activities of Du-145. PC-3, and 1-LN-PC-3-1A human prostate tumors grown in nude mice: correlation with tumor invasive behavior. Cell. Mol. Biol. Res., *39:* 751–760, 1993.

9. Kwaan, H. C., Keer, H. N., Radosevich, J. A., Cajot, J. F., and Ernst, R. Components of the plasminogen-plasmin system in human tumor cell lines. Semin. Thromb. Hemost., *17:* 175–182, 1991.

10. Kwaan, H. C., and Keer, H. N. Fibrinolysis and cancer. Semin. Thromb. Hemost., *16:* 230–235, 1990.

11. Jankun, J., Maher, V. M., and McCormick, J. J. Malignant transformation of human fibroblasts correlates with increased activity of receptor-bound plasminogen activator. Cancer Res., *51:* 1221–1226, 1991.

12. Jankun, J., Merrick, H. W., and Goldblatt, P. J. Expression and localization of elements of the plasminogen activation system in benign breast disease and breast cancers. J. Cell. Biochem., *53:* 135–144, 1993.

13. Billstrom, A., Lecander, I., Dagnaes-Hansen, F., Dahllof, B., Stenram, U., and Hartley-Asp, B. Differential expression of uPA in an aggressive (DU 145) and a nonaggressive (1013L) human prostate cancer xenograft. Prostate, *26:* 94–104, 1995.

14. Jankun, J., Keck, R. W., Skrzypczak-Jankun, E., and Swiercz, R. Inhibitors of urokinase reduce size of prostate cancer xenografts in severe combined immunodeficient mice. Cancer Res., *57:* 559–563, 1997.

15. Magdolen, V., Arroyo de Prada, N., Sperl, S., Muehlenweg, B., Luther, T., Wilhelm, O. G., Magdolen, U., Graeff, H., Reuning, U., and Schmitt, M. Natural and synthetic inhibitors of the tumor-associated serine protease urokinase-type plasminogen activator. Adv. Exp. Med. Biol., *477:* 331–341, 2000.

16. Evans, D. M., and Sloan-Stakleff, K. Suppression of the invasive capacity of human breast cancer cells by inhibition of urokinase plasminogen activator via amiloride and B428. Am. Surg., *66:* 460–464, 2000.

17. Jankun, J., and Skrzypczak-Jankun, E. Molecular basis of specific inhibition of urokinase plasminogen activator by amiloride. Cancer Biochem. Biophys., *17:* 109–123, 1999.

18. Kellen, J. A., Mirakian, A., and Kolin, A. Antimetastatic effect of amiloride in an animal tumour model. Anticancer Res., *8:* 1373–1376, 1988.

19. Swiercz, R., Keck, R. W., Skrzypczak-Jankun, E., Selman, S. H., and Jankun, J. Recombinant PAI-1 inhibits angiogenesis and reduces size of LNCaP prostate cancer xenografts in SCID mice. Oncol. Rep., *8:* 463–470, 2001.

20. Bajou, K., Masson, V., Gerard, R. D., Schmitt, P. M., Albert, V., Praus, M., Lund, L. R., Frandsen, T. L., Brunner, N., Dano, K., Fusenig, N. E., Weidle, U., Carmeliet, G., Loskutoff, D., Collen, D., Carmeliet, P., Foidart, J. M., and Noel, A. The plasminogen activator inhibitor PAI-1 controls *in vivo* tumor vascularization by interaction with proteases, not vitronectin. Implications for antiangiogenic strategies. J. Cell Biol., *152:* 777–784, 2001.

21. Tucker, H. M., Mottonen, J., Goldsmith, E. J., and Gerard, R. D. Engineering of plasminogen activator inhibitor-1 to reduce the rate of latency transition. Nat. Struct. Biol., *2:* 442–445, 1995.

22. Sharp, A. M., Stein, P. E., Pannu, N. S., Carrell, R. W., Berkenpas, M. B., Ginsburg, D., Lawrence, D. A., and Read, R. J. The active conformation of plasminogen activator inhibitor 1, a target for drugs to control fibrinolysis and cell adhesion. Struct. Fold Des., *7:* 111–118, 1999.

23. Schwede, T., Diemand, A., Guex, N., and Peitsch, M. C. Protein structure computing in the genomic era. Res. Microbiol., *151:* 107–112, 2000.

24. Guex, N., Diemand, A., and Peitsch, M. C. Protein modelling for all. Trends Biochem. Sci., *24:* 364–367, 1999.

25. Sanger, F. Determination of nucleotide sequences in DNA. Science (Wash. DC), *214:* 1205–1210, 1981.

26. Berkenpas, M. B., Lawrence, D. A., and Ginsburg, D. Molecular evolution of plasminogen activator inhibitor-1 functional stability. EMBO J., *14:* 2969–2977, 1995.

27. Shaw, A., and Bott, R. Engineering enzymes for stability. Curr. Opin. Struct. Biol., *6:* 546–550, 1996.

28. Ivens, A., Mayans, O., Szadkowski, H., Jurgens, C., Wilmanns, M., and Kirschner, K. Stabilization of a ($\beta\alpha$)8-barrel protein by an engineered disulfide bridge. Eur. J. Biochem., *269:* 1145–1153, 2002.

29. Strandberg, L., Lawrence, D. A., Johansson, L. B., and Ny, T. The oxidative inactivation of plasminogen activator inhibitor type 1 results from a conformational change in the molecule and does not require the involvement of the P1′ methionine. J. Biol. Chem., *266:* 13852–13858, 1991.

30. Picone, D., Crescenzi, O., Angeli, S., Marchese, S., Brandazza, A., Ferrara, L., Pelosi, P., and Scaloni, A. Bacterial expression and conformational analysis of a chemosensory protein from *Schistocerca gregaria*. Eur. J. Biochem., *268:* 4794–4801, 2001.

31. Ronnmark, J., Hansson, M., Nguyen, T., Uhlen, M., Robert, A., Stahl, S., and Nygren, P. A. Construction and characterization of affibody-Fc chimeras produced in *Escherichia coli*. J. Immunol. Methods, *261:* 199–211, 2002.

32. Gibson, L. C., Jensen, P. E., and Hunter, C. N. Magnesium chelatase from Rhodobacter sphaeroides: initial characterization of the enzyme using purified subunits and evidence for a BchI-BchD complex. Biochem. J., *337:* 243–251, 1999.

33. Gils, A., and Declerck, P. J. Proteinase specificity and functional diversity in point mutants of plasminogen activator inhibitor 1. J. Biol. Chem., *272:* 12662–12666, 1997.

34. Wagner, O. F., de Vries, C., Hohmann, C., Veerman, H., and Pannekoek, H. Interaction between plasminogen activator inhibitor type 1 (PAI-1) bound to fibrin and either tissue-type plasminogen activator (t-PA) or urokinase-type plasminogen activator (u-PA). Binding of t-PA/PAI-1 complexes to fibrin mediated by both the finger and the kringle-2 domain of t-PA. J. Clin. Investig., *84:* 647–655, 1989.

35. Lawrence, D., Strandberg, L., Grundstrom, T., and Ny, T. Purification of active human plasminogen activator inhibitor 1 from *Escherichia coli*. Comparison with natural and recombinant forms purified from eucaryotic cells. Eur. J. Biochem., *186:* 523–533, 1989.

36. Sherman, P. M., Lawrence, D. A., Yang, A. Y., Vandenberg, E. T., Paielli, D., Olson, S. T., Shore, J. D., and Ginsburg, D. Saturation mutagenesis of the plasminogen activator inhibitor-1 reactive center. J. Biol. Chem., *267:* 7588–7595, 1992.

37. Alessi, M. C., Declerck, P. J., De Mol, M., Nelles, L., and Collen, D. Purification and characterization of natural and recombinant human plasminogen activator inhibitor-1 (PAI-1). Eur. J. Biochem., *175:* 531–540, 1988.

38. McMahon, G. A., Petitclerc, E., Stefansson, S., Smith, E., Wong, M. K., Westrick, R. J., Ginsburg, D., Brooks, P. C., and Lawrence, D. A. Plasminogen activator inhibitor-1 regulates tumor growth and angiogenesis. J. Biol. Chem., *276:* 33964–33968, 2001.

39. Bajou, K., Noel, A., Gerard, R. D., Masson, V., Brunner, N., Holst-Hansen, C., Skobe, M., Fusenig, N. E., Carmeliet, P., Collen, D., and Foidart, J. M. Absence of host plasminogen activator inhibitor 1 prevents cancer invasion and vascularization. Nat. Med., *4:* 923–928, 1998.

40. Stefansson, S., Petitclerc, E., Wong, M. K., McMahon, G. A., Brooks, P. C., and Lawrence, D. A. Inhibition of angiogenesis *in vivo* by plasminogen activator inhibitor-1. J. Biol. Chem., *276:* 8135–8141, 2001.

41. Ignjatovic, Z., and Nikolic, L. Inhibition of angiogenesis in the cornea with amiloride (in Serbian). Srp. Arh. Celok. Lek., *124:* 120–123, 1996.

A Novel Form of the Plasminogen Activator Inhibitor Created by Cysteine Mutations Extends Its Half-Life: Relevance to Cancer and Angiogenesis[1]

Joanna Chorostowska-Wynimko, Rafal Swiercz, Ewa Skrzypczak-Jankun, et al.

Updated version	Access the most recent version of this article at: http://mct.aacrjournals.org/content/2/1/19

Cited articles	This article cites 38 articles, 11 of which you can access for free at: http://mct.aacrjournals.org/content/2/1/19.full#ref-list-1
Citing articles	This article has been cited by 2 HighWire-hosted articles. Access the articles at: http://mct.aacrjournals.org/content/2/1/19.full#related-urls

E-mail alerts	Sign up to receive free email-alerts related to this article or journal.
Reprints and Subscriptions	To order reprints of this article or to subscribe to the journal, contact the AACR Publications Department at pubs@aacr.org.
Permissions	To request permission to re-use all or part of this article, use this link http://mct.aacrjournals.org/content/2/1/19. Click on "Request Permissions" which will take you to the Copyright Clearance Center's (CCC) Rightslink site.